ADVANCED FUNCTIONAL MATERIALS

Supporting Information

for *Adv. Funct. Mater.*, DOI 10.1002/adfm.202312773

Mechanistic Insights of Zn-Ion Storage in Synergistic Vanadium-Based Composites

Lingli Xing, Xinyu Zhang, Nuo Xu, Ping Hu, Kun Wang* and Qinyou An**

Mechanistic Insights of Zn-ion Storage in Synergistic Vanadium-based Composites

Lingli Xing[a], Xinyu Zhang[a], Nuo Xu[a], Ping Hu[b,d,], Kun Wang[c,*], Qinyou An[a,b,*]*

[a] State Key Laboratory of Advanced Technology for Materials Synthesis and Processing, Wuhan University of Technology, Wuhan, 430070, P. R. China

[b] Hubei Longzhong Laboratory, Wuhan University of Technology (Xiangyang Demonstration Zone), Xiangyang, 441000, P. R. China

[c] State Key Laboratory of Silicate Materials for Architectures, Wuhan University of Technology, Wuhan, 430070, P. R. China

[d] School of Microelectronics, Hubei University, Wuhan, 430062, P. R. China

E-mail: huping316@163.com; kun.wang@whut.edu.cn; anqinyou86@whut.edu.cn

4.2. Electrochemical measurements

Zinc foils as the anode, $Zn(CF_3SO_3)_2$ as electrolyte, glass microfiber filter (Whatman, GF/D grade) as a separator, CR2025 coin-type cell assembly. A working electrode consists of 70 wt% NVO-AVO, 20 wt% acetylene black, and 10 wt% polyvinylidene fluoride (PVDF). Galvanostatic discharge/charge tests were carried out using a NEWARE battery test system (CT-4008T-5V10mA-164, Shenzhen China). Galvanostatic intermittent titration technique (GITT) curve was performed at a multichannel battery testing system (LAND CT2001A). Cyclic voltammograms (CV) and electrochemical impedance spectroscopy (EIS) were obtained on an Auto lab

PGSTAT302 N.

4.3. Material characterization

X-ray diffraction (XRD) was measured using a Bruker D8 Discover X-ray diffractometer with the non-monochromatic Cu Kα X-ray as the source (λ = 1.5406 Å). Raman spectra were captured with a HORIBA LabRAM HR Evolution micro-Raman spectroscopy system with an excitation laser wavelength of λ = 532 nm. Fourier transforms infrared (FTIR) spectra were captured with a Nicolet 6700 (Thermo Fisher Scientific Co., USA) IR spectrometer. Thermogravimetric analysis (TGA) curves were performed using a Netzsch STA 449C simultaneous analyzer. Brunauer-Emmett-Teller (BET) surface area was collected through Tristar II 3020 instrument at 77 K. X-ray photoelectron spectroscopy (XPS) spectra were carried out on a VG Multi Lab 2000 instrument. Scanning electron microscopy (SEM) images were obtained using a JEOL-7100F scanning electron microscope. Transmission electron microscopy (TEM) and high-resolution TEM (HRTEM) images were captured with a JEM-2100F STEM/EDS microscope.

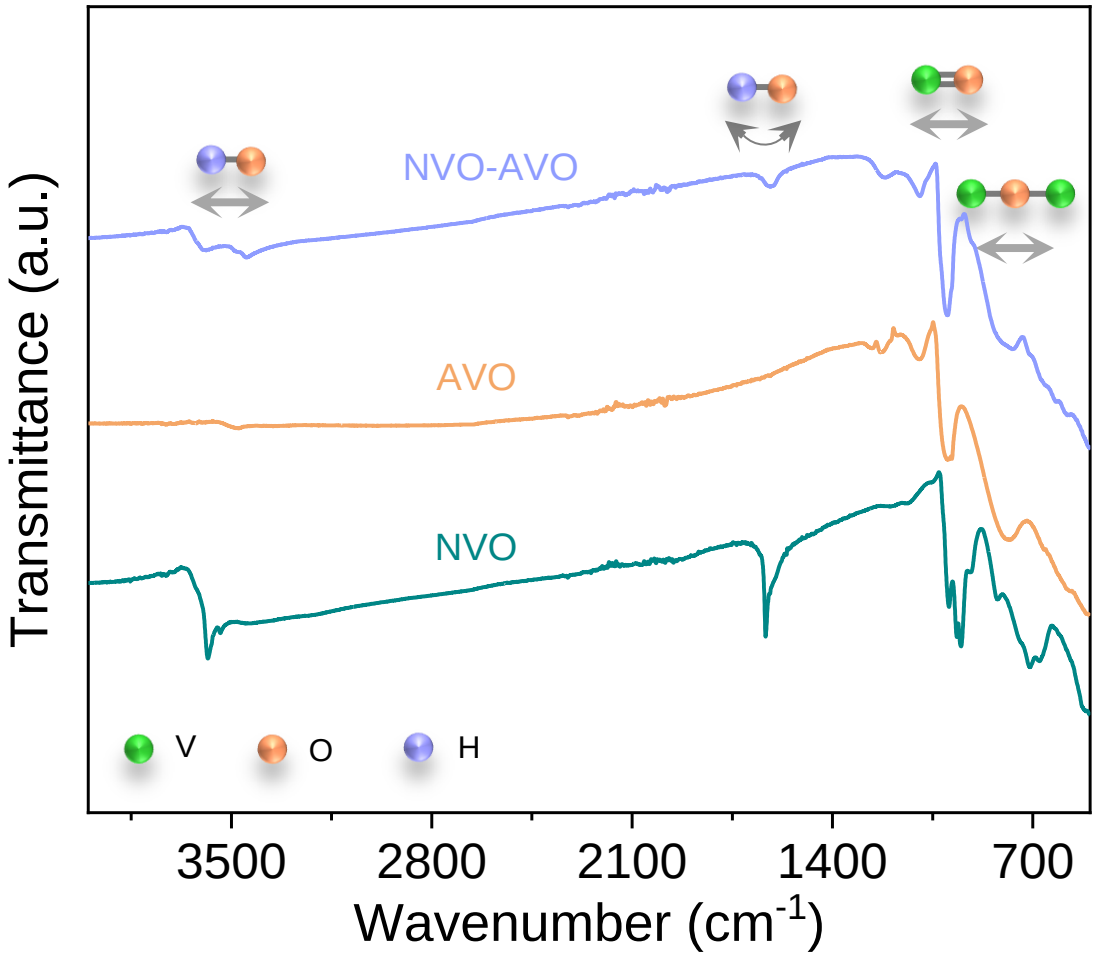

Figure S1. FTIR spectra of the three active materials.

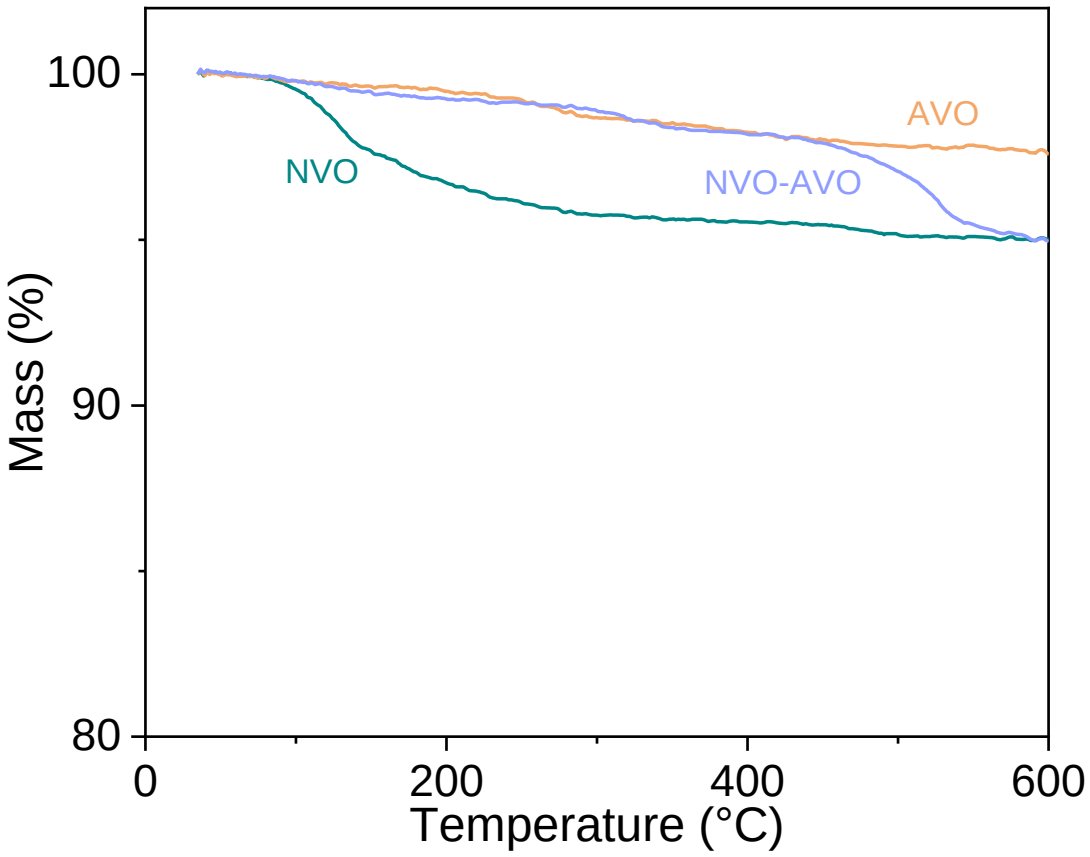

Figure S2. TGA curves of the three active materials.

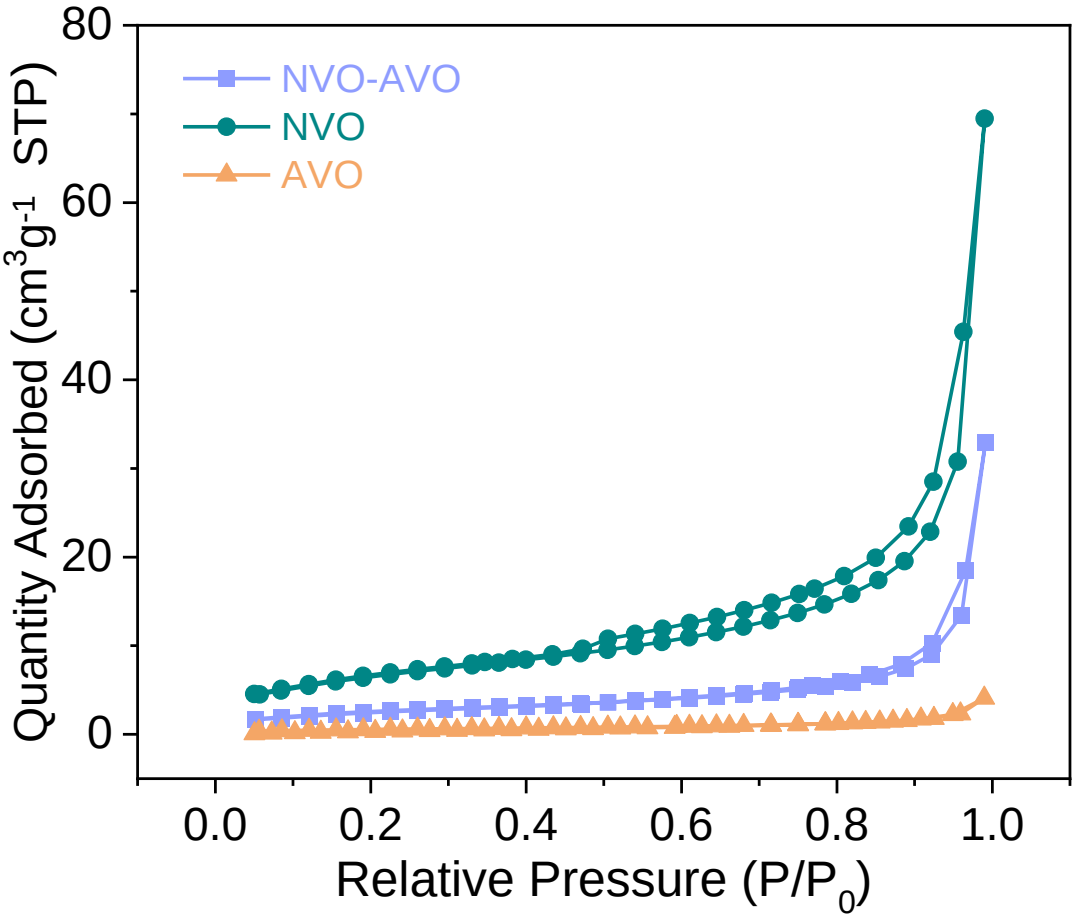

Figure S3. N_2 adsorption-desorption isotherms of the three active materials.

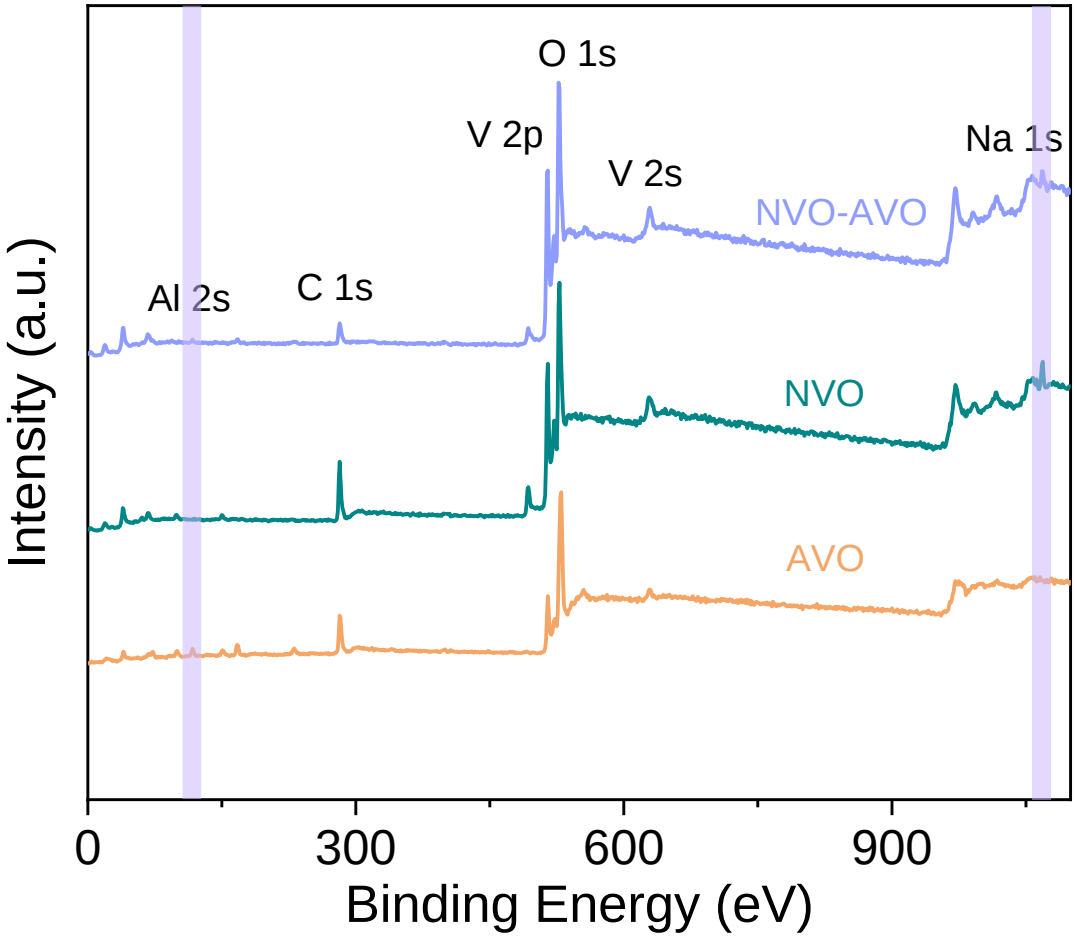

Figure S4. XPS survey spectra of the three active materials.

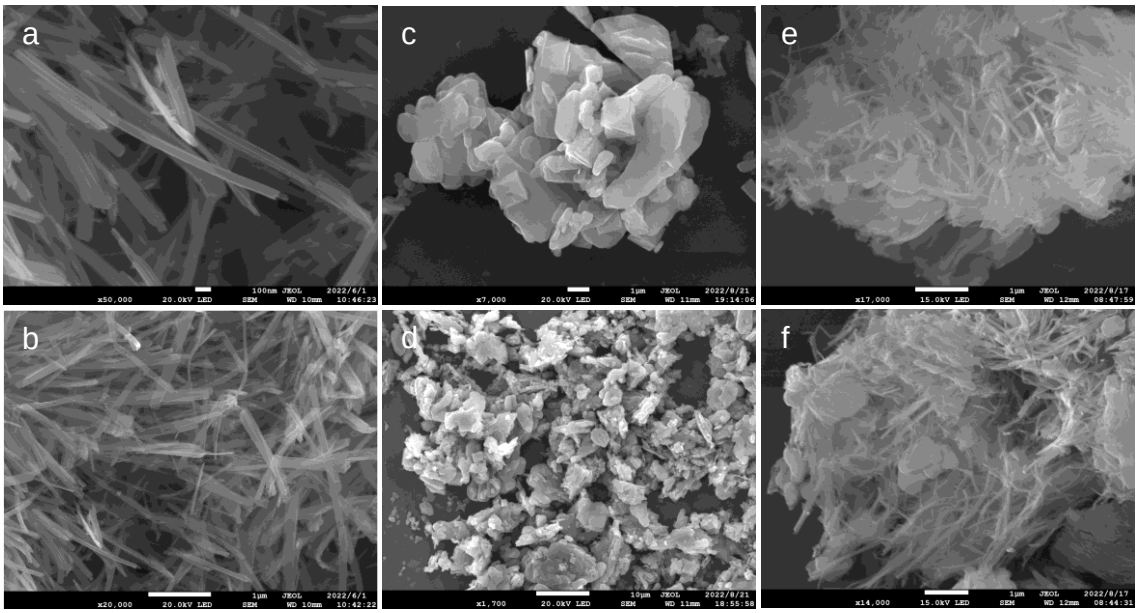

Figure S5. Typical SEM images of NVO (a, b), AVO (c, d) and NVO-AVO (e, f).

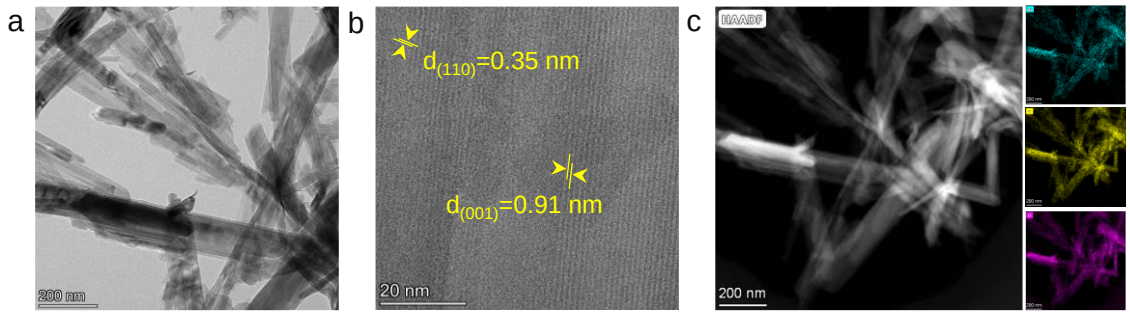

Figure S6. (a) TEM image, (b) HRTEM image, (c) HAADF image and corresponding Na, V, O element mapping of NVO.

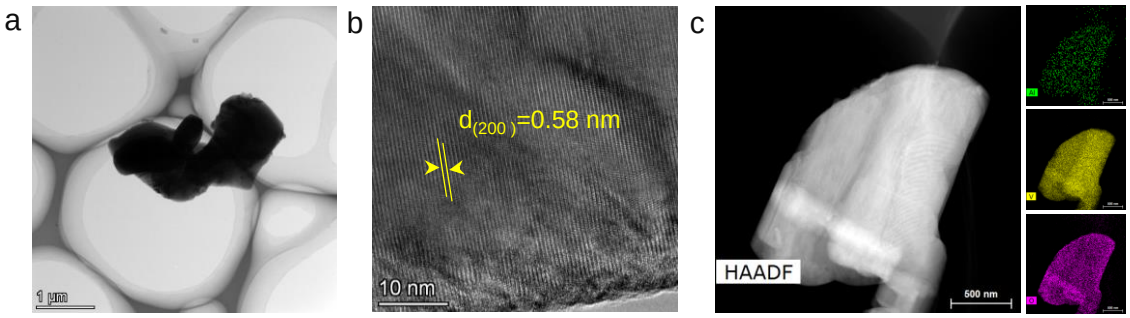

Figure S7. (a) TEM image, (b) HRTEM image, (c) HAADF image and corresponding Al, V, O element mapping of AVO.

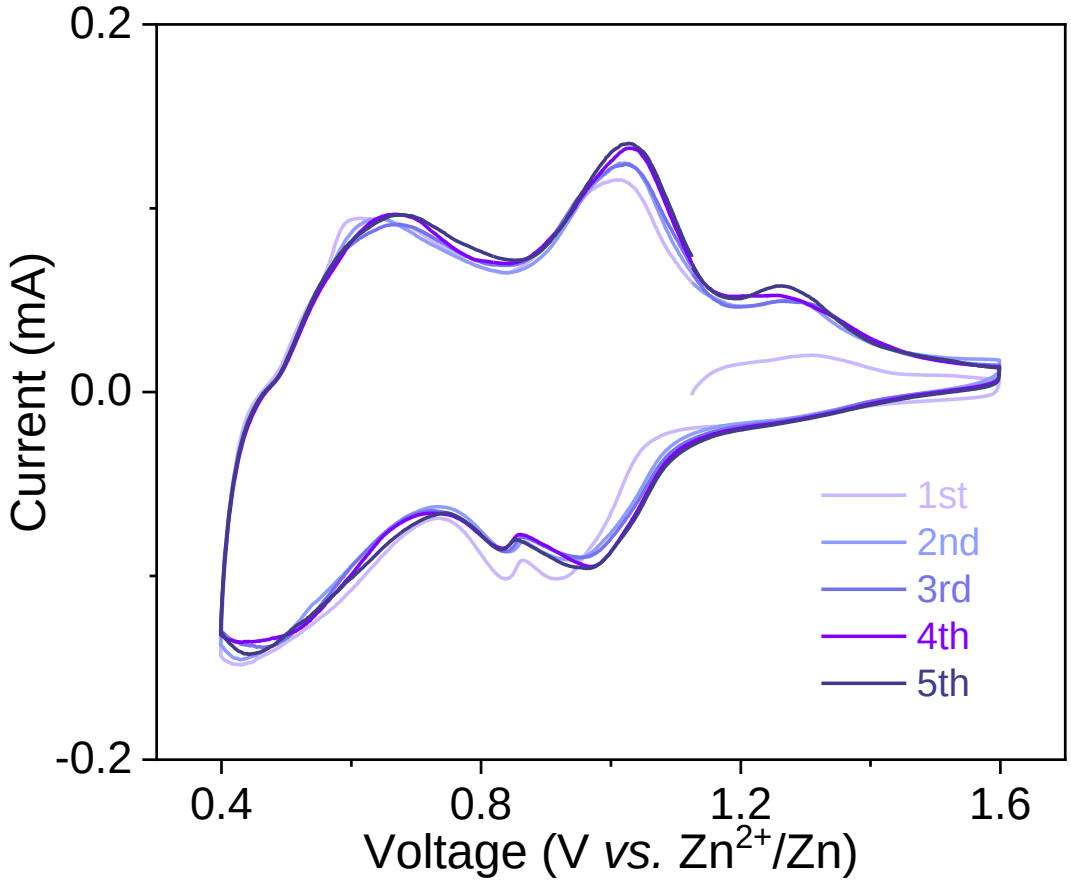

Figure S8. CV curves of the initial five cycles of NVO-AVO cathode.

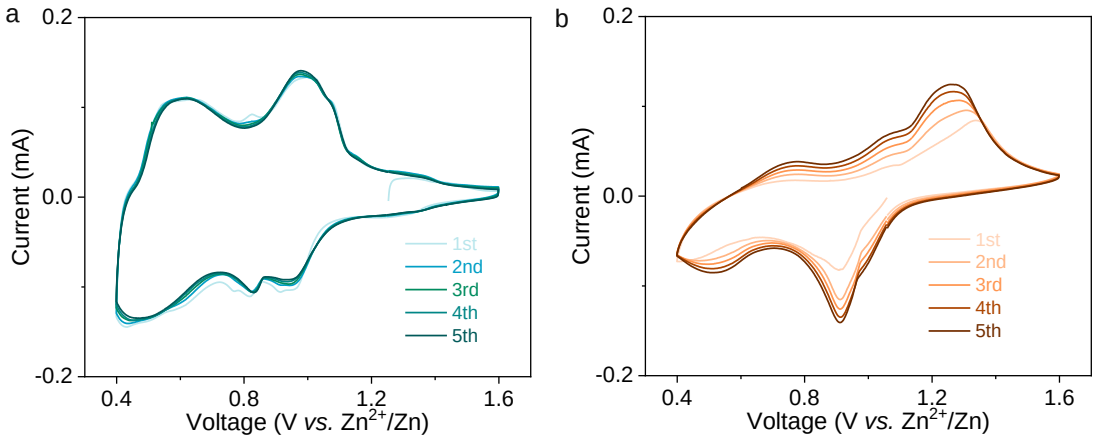

Figure S9. CV curves of the initial five cycles of NVO (a) and AVO (b) cathode.

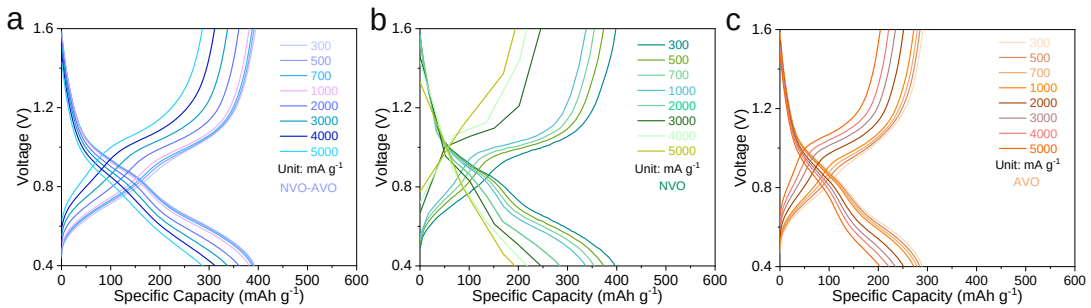

Figure S10. Representative charge/discharge curves for the three active materials at different current densities.

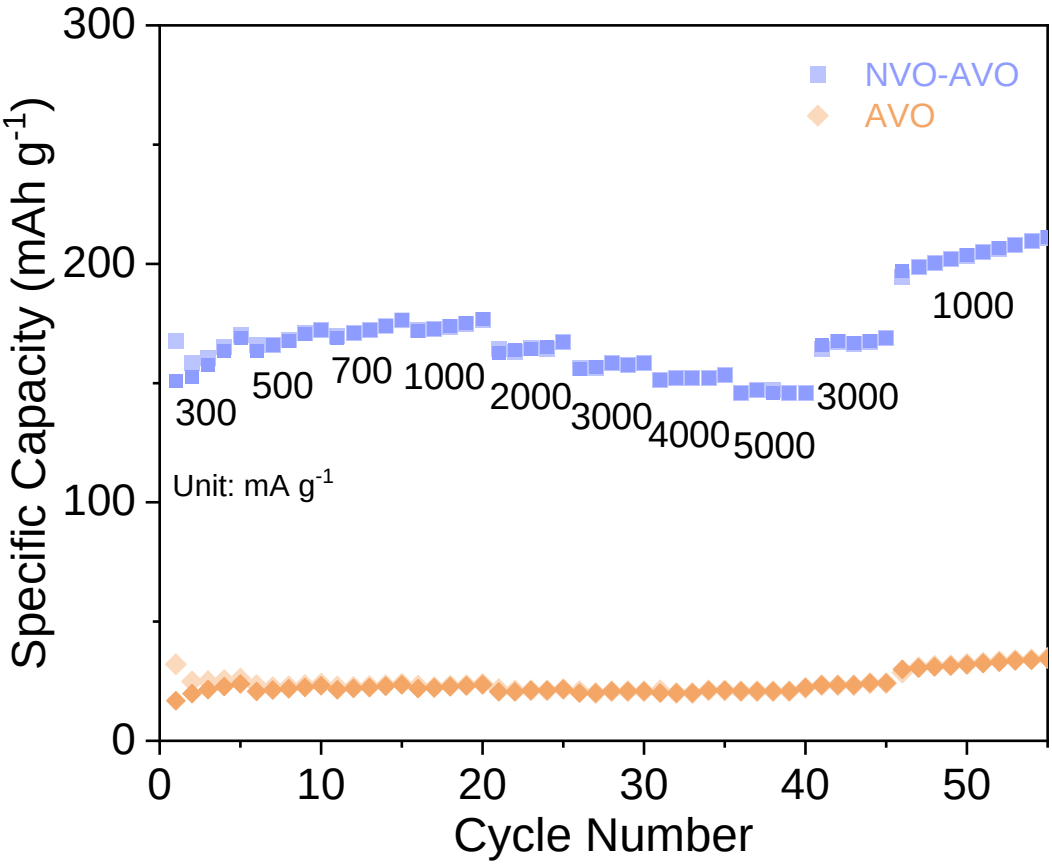

Figure S11. Rate performance at various current densities without pre-cycled.

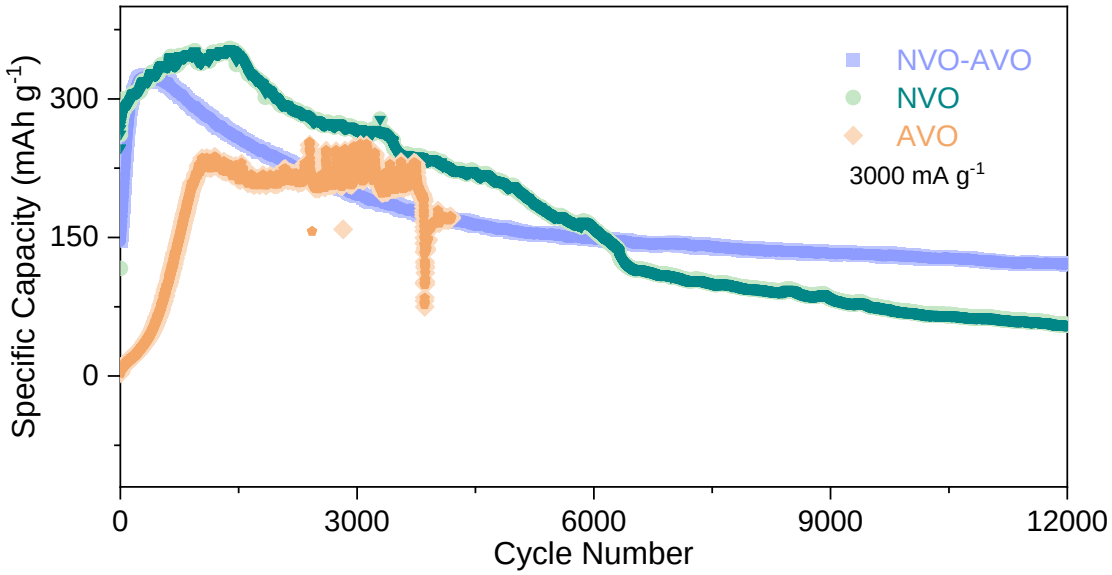

Figure S12. Long-term cycling stability at 3000 mA g^{-1} of the three active materials.

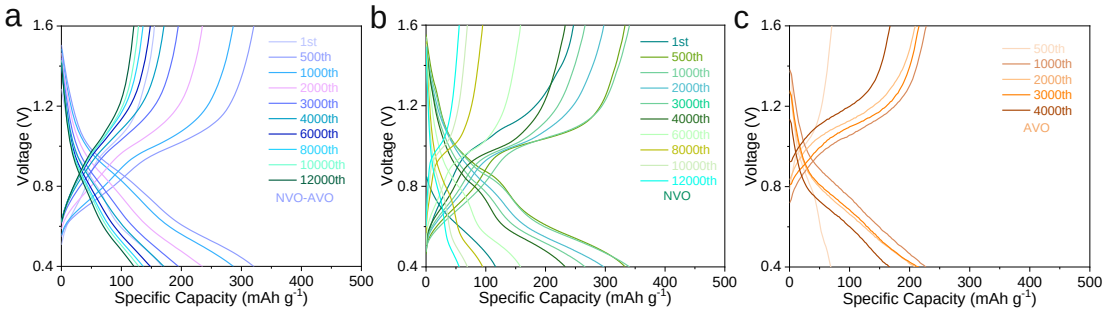

Figure S13. Representative charge/discharge curves for the three active materials at 3000 mA g^{-1}.

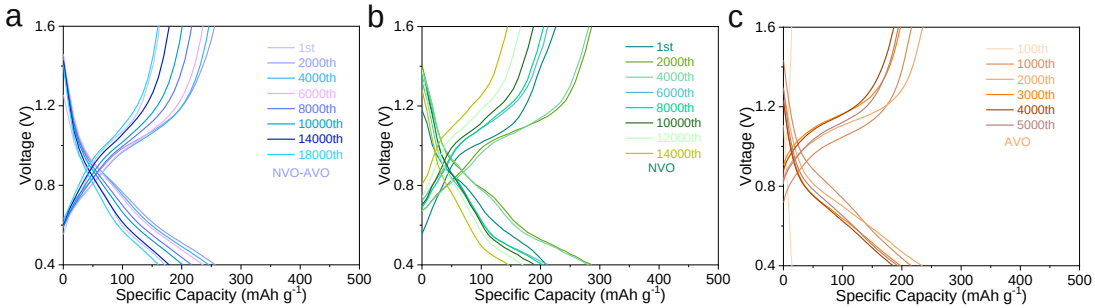

Figure S14. Representative charge/discharge curves for the three active materials at 5000 mA g^{-1}.

Table S1. Comparison of the electrochemical performance between this work and some representative cathode materials in AZIBs.

Materials	Cycling performance	Specific capacity (mA h g^{-1} at mA g^{-1})	Ref.
NVO-AVO	270/18300/5000	382 (1000 mA g^{-1})	This work
$Na_2V_6O_{16}·3H_2O$	142/5000/5000	302 (1000 mA g^{-1})	[1]
$(NH_4)_2V_{10}O_{25}·8H_2O$	183/1000/2000	240 (1000 mA g^{-1})	[2]
$NaV_3O_8·1.5H_2O$	150/1000/4000	240 (1000 mA g^{-1})	[3]
$KV_3O_8·0.75H_2O$/MWCNTs	201/500/1000	205 (1000 mA g^{-1})	[4]
$Na_{1.25}V_3O_8$	78/50/1000	80 (1000 mA g^{-1})	[5]
$Al_xV_2O_5·nH_2O$	208/2000/5000	255 (1000 mA g^{-1})	[6]
$V_2O_5·nH_2O$	200/1000/5000	253 (1000 mA g^{-1})	[7]
NaV_3O_8	150/2000/400	98 (1000 mA g^{-1})	[8]
$Co_xV_2O_5·nH_2O$	188/1000/5000	265 (1000 mA g^{-1})	[9]
$Na_{1.1}V_3O_{7.9}$	134/1000/5000	125 (1000 mA g^{-1})	[10]

Note: Cycling performance: capacity/cycle number/rate.

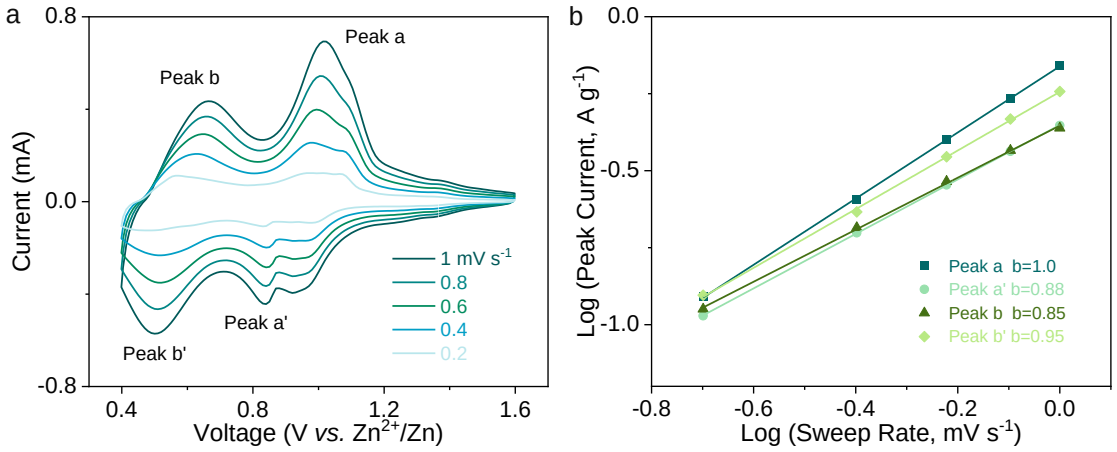

Figure S15. (a) CV curves of NVO at different scan rates. (b) The plots of log (peak current) versus log (sweep rate) at each peak from CV curves of NVO.

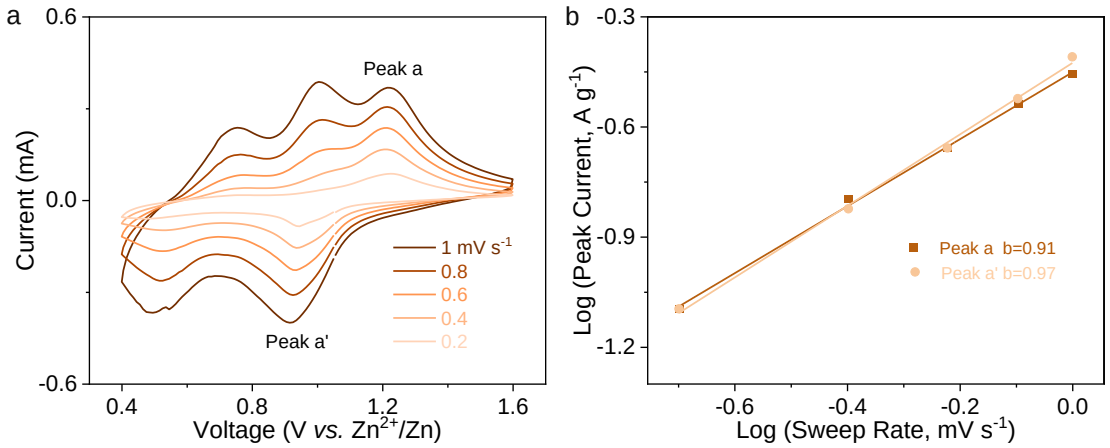

Figure S16. (a) CV curves of AVO at different scan rates. (b) The plots of log (peak current) versus log (sweep rate) at each peak from CV curves of AVO.

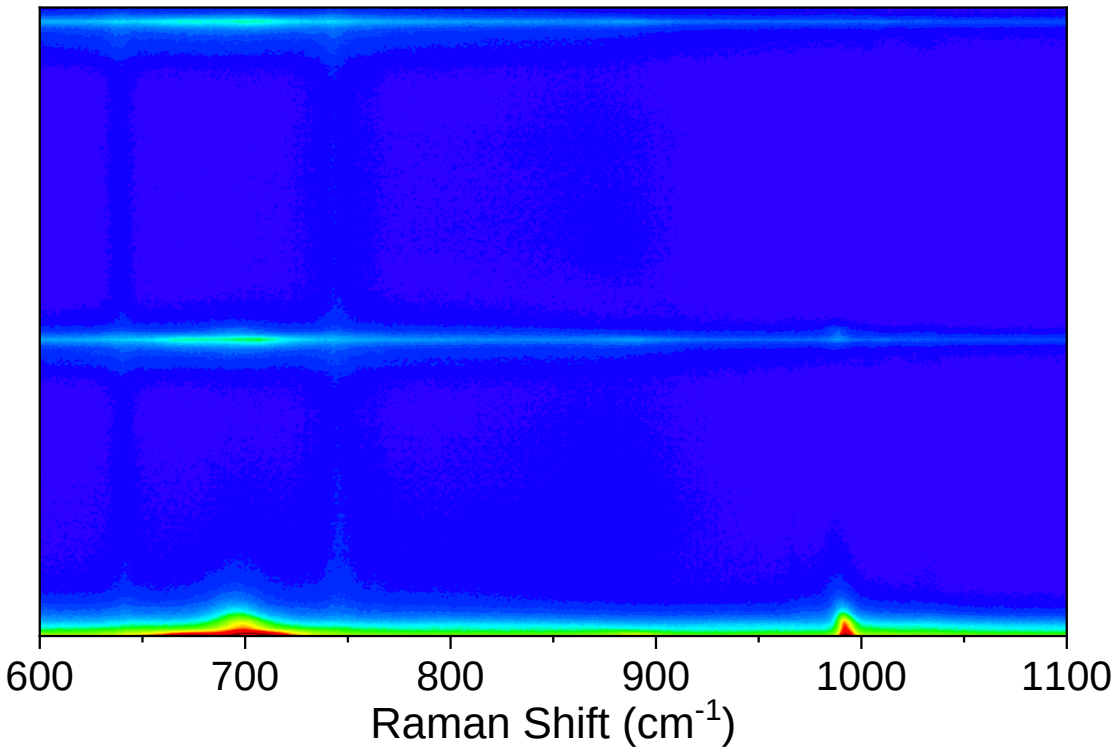

Figure S17. Enlarged *in-situ* Raman spectra from 600 cm^{-1} to 1100 cm^{-1} of NVO-AVO.

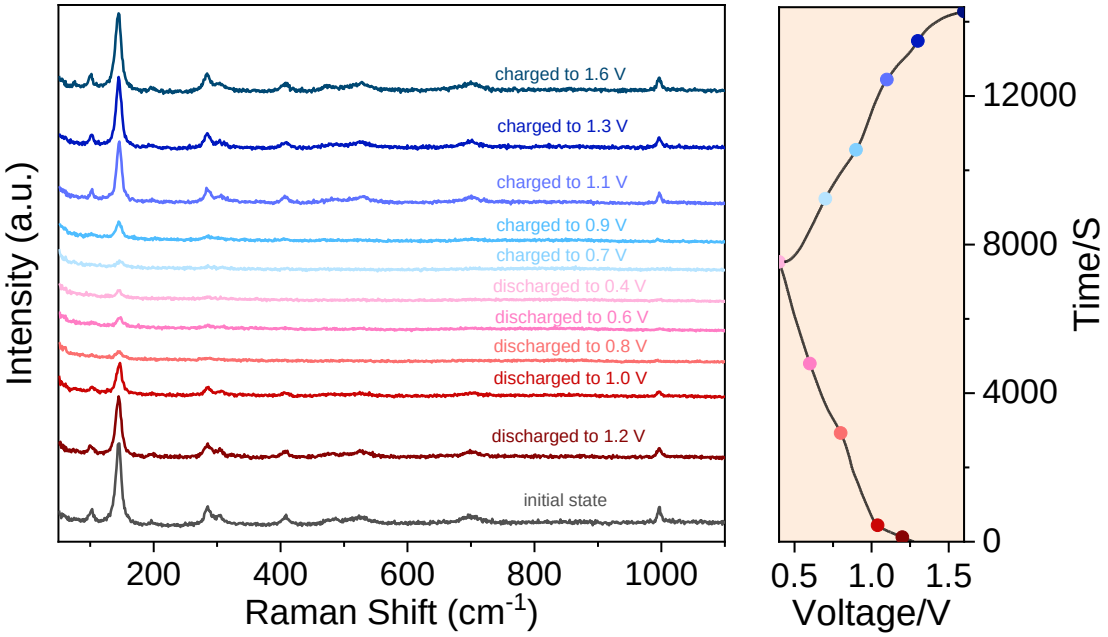

Figure S18. *Ex-situ* Raman spectra of NVO-AVO.

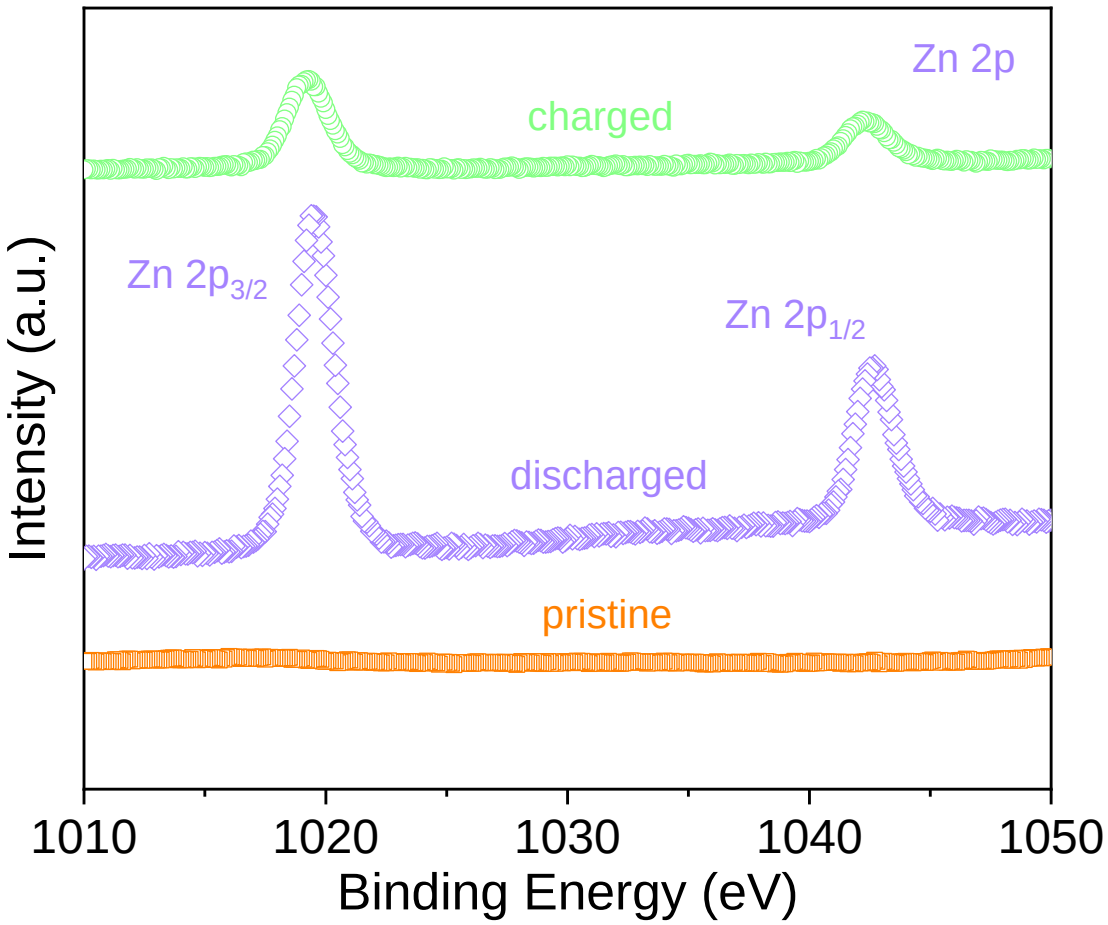

Figure S19. *Ex-situ* XPS spectra of Zn 2p of NVO-AVO.

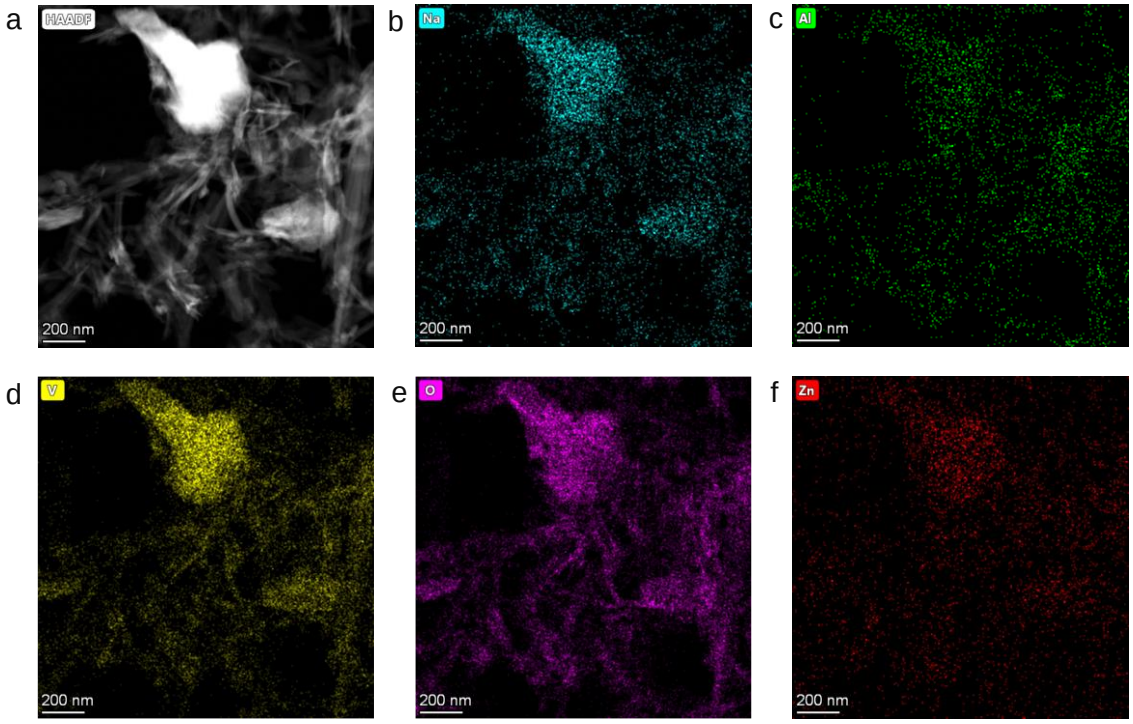

Figure S20. (a) HAADF image and (b-f) the corresponding element distribution maps of NVO-AVO electrode in pristine.

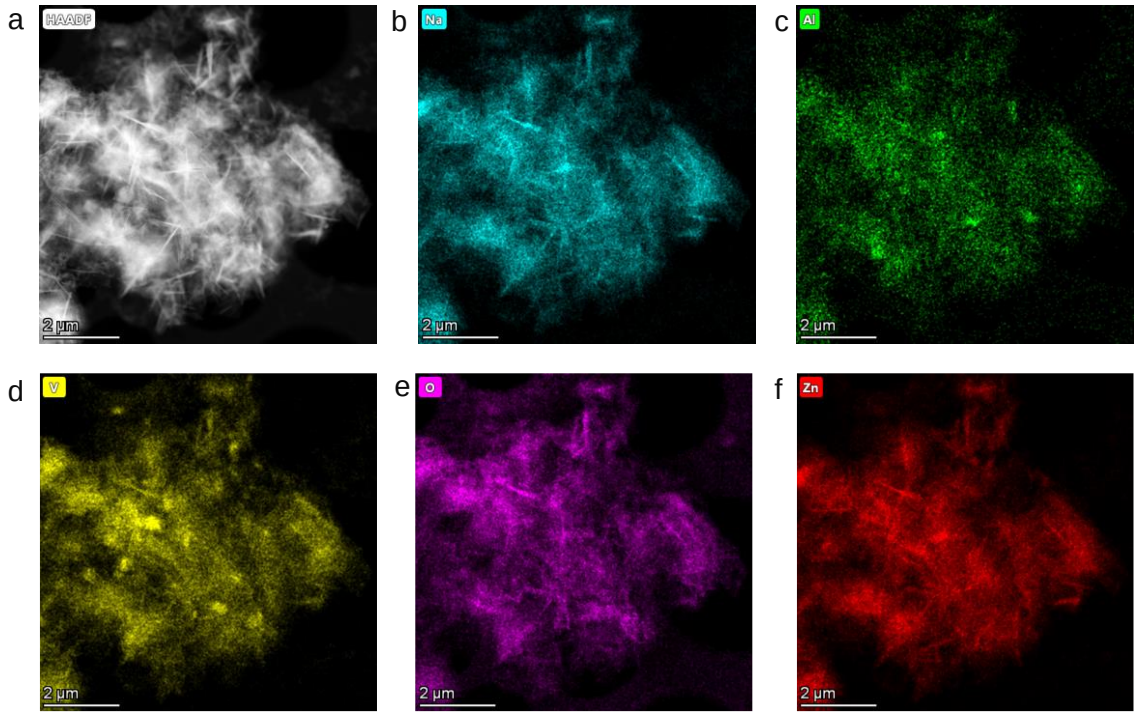

Figure S21. (a) HAADF image and (b-f) the corresponding element distribution maps of the fully discharged NVO-AVO electrode.

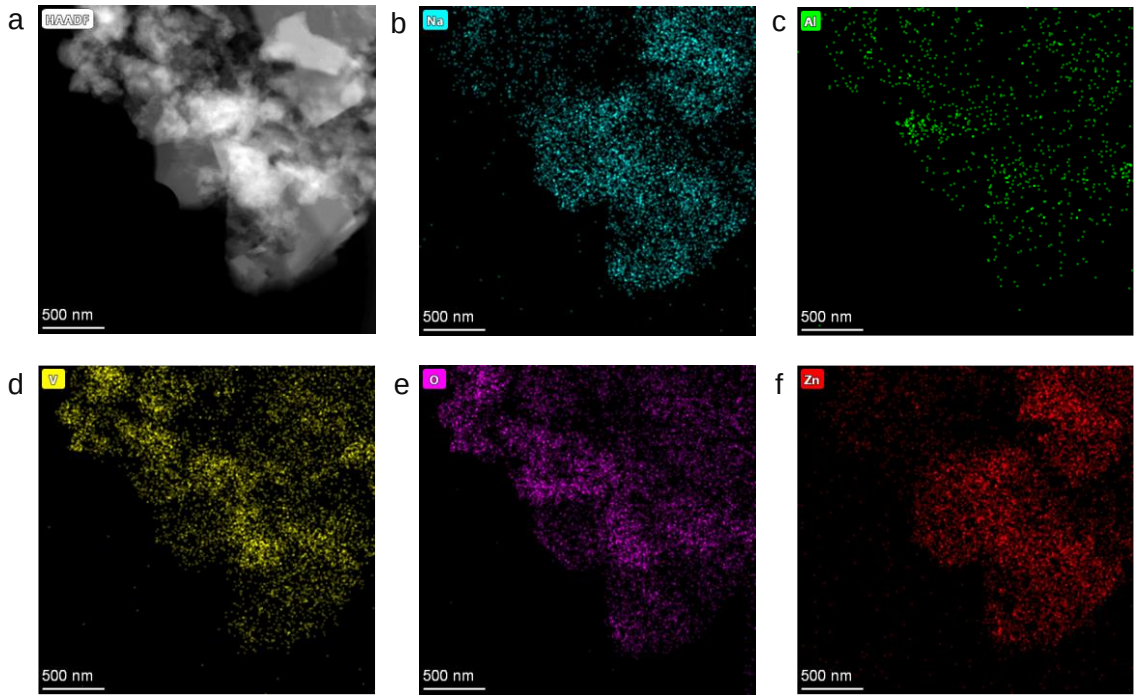

Figure S22. (a) HAADF image and (b-f) the corresponding element distribution maps of the fully charged NVO-AVO electrode.

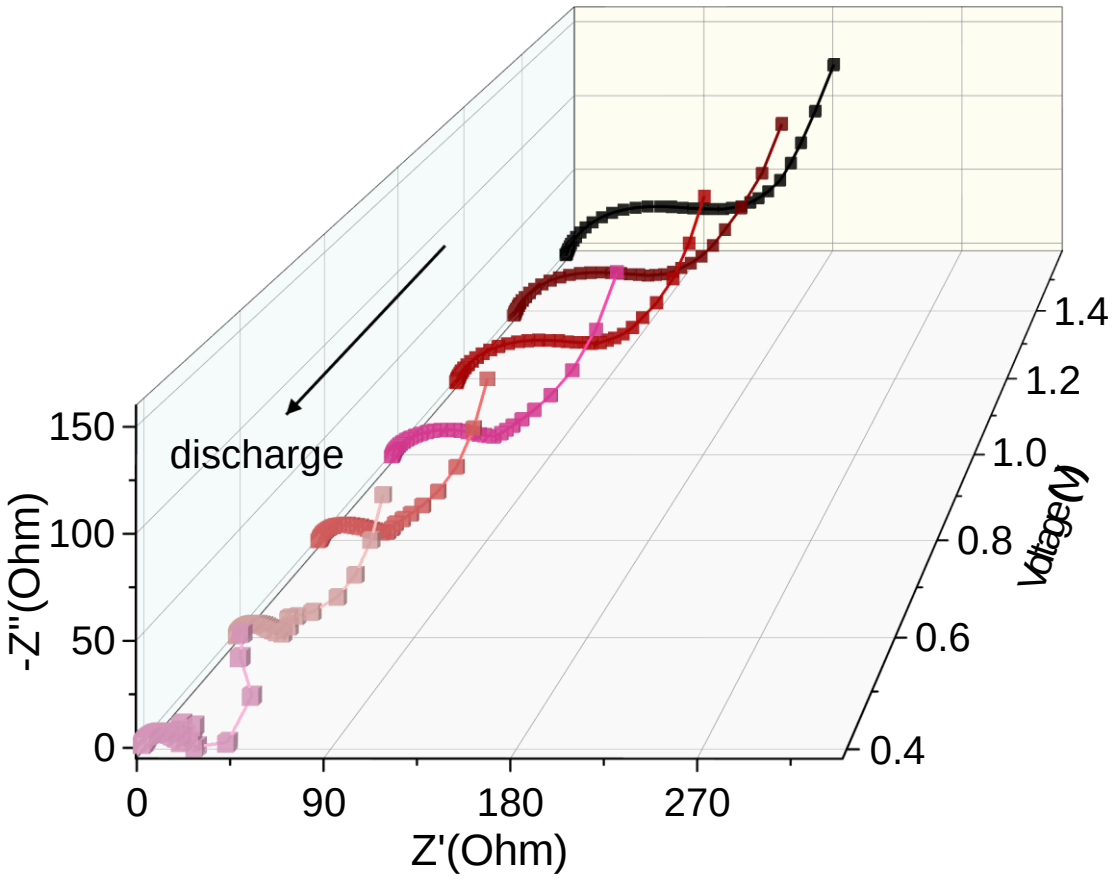

Figure S23. *In-situ* impedance spectra of NVO-AVO cathode at 100 mA g^{-1} during the first discharge process.

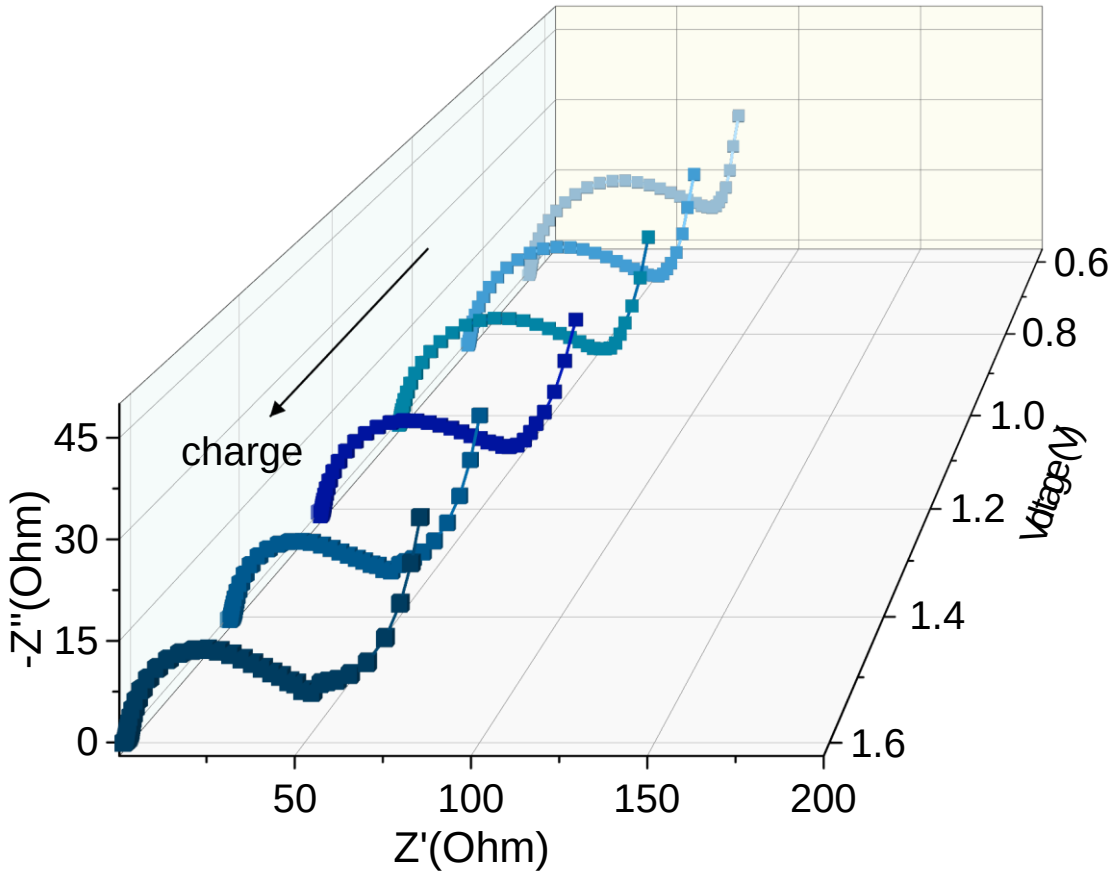

Figure S24. *In-situ* impedance spectra of NVO-AVO cathode at 100 mA g^{-1} during the first charge process.

References

[1] H. T. Tan, D. Chen, W. L. Liu, C. T. Liu, B. Lu, X. H. Rui, Q. Y. Yan, *Batteries Supercaps* **2020**, *3*, 254.

[2] H. M. Jiang, Y. F. Zhang, Y. Y. Liu, J. Yang, L. Xu, P. Wang, Z. M. Gao, J. Q. Zheng, C. G. Meng, Z. H. Pan, *J. Mater. Chem. A* **2020**, *8*, 15130.

[3] F. Wan, L. L. Zhang, X. Dai, X. Y. Wang, Z. Q. Niu, J. Chen, *Nat. Commun.* **2018**, *9*, 1656.

[4] F. Wan, S. Huang, H. M. Cao, Z. Q. Niu, *ACS Nano* **2020**, *14*, 6752.

[5] S. J. Kim, C. R. Tang, G. Singh, L. M. Housel, S. Z. Yang, K. J. Takeuchi, A. C. Marschilok, E. S. Takeuchi, Y. M. Zhu, *Chem. Mater.* **2020**, *32*, 2053.

[6] F. Wan, Z. M. Hao, S. Wang, Y. X. Ni, J. C. Zhu, Z. W. Tie, S. S. Bi, Z. Q. Niu, J. Chen, *Adv. Mater.* **2021**, *33*, 2102701.

[7] M. Tian, C. F. Liu, J. Q. Zheng, X. X. Jia, E. P. Jahrman, G. T. Seidler, D. H. Long, M. Atif, M. Alsalhi, G. Z. Cao, *Energy Storage Mater.* **2020**, *29*, 9.

[8] X. Q. Shan, S. Kim, A. M. M. Abeykoon, G. Kwon, D. Olds, X. W. Teng, *ACS Appl. Mater. Interfaces* **2020**, *12*, 54627.

[9] W. C. Leng, X. Liu, Y. Gong, *Chem. Eng. J.* **2022**, *431*, 134034.

[10] B. H. She, L. T. Shan, H. J. Chen, J. Zhou, X. Guo, G. Z. Fang, X. X. Cao, S. Q. Liang, *J. Energy Chem.* **2019**, *37*, 172.